

# Focus Measure in a Liquid-filled Diaphragm (LFD) Lens Using Passive Auto-focus Method

S.J. Abdullah, M.M. Ratnam, Z. Samad  
School of Mechanical Engineering  
Engineering Campus, Universiti Sains Malaysia  
14300 Nibong Tebal, Malaysia  
E-mail: mmaran@eng.usm.my

**Abstract**— Auto-focusing in imaging systems depends on the determination of the correct image focus criterion. In this research, the image captured by a liquid-filled diaphragm (LFD) fluid lens was analyzed to determine a focus measure criterion that can be used to establish the correct focus and thus quantify the image quality. The LFD lens was actuated using a stepper-motor driven syringe mechanism. The lens diaphragm was made of polydimethylsiloxane (PDMS) polymer that exhibit good optical properties. The lens focal length was controlled by varying the fluid volume within the diaphragm lens. A CCD camera was attached to the fluid lens to capture live images of a binary target. The edge slope width (ESW) of the pixel intensity profile across the white-to-black transition region in a binary target was used as the focus measure. The experiments carried out showed the viability of the proposed focus measure criterion for automatically focusing the image formed by a diaphragm-type fluid lens.

**Keywords**—liquid-fill, diaphragm, lens, focus

## I. INTRODUCTION

Optical devices such as cameras, microscopes and other imaging systems use various types of variable focusing mechanisms that have been developed in the past. The conventional methods of varying the lens focal length, i.e. by using motors, slides and gears, is still widely used in most imaging systems. The main disadvantage of the conventional focusing mechanism is that it requires several interlinking mechanical components. The inherent contact-friction subjects these components to wear, thus affecting the focus quality of the captured images. Since there is a general advancement towards making smaller cameras and imaging systems, accommodating the various moving parts in the conventional focusing mechanism faces space and manufacturing constraints. Therefore, a new focusing mechanism with fewer moving parts is required for enhancing the performance of optical devices.

Fluid lenses have great potential for replacing the traditional glass lenses in achieving variable focusing. In a fluid lens system a single lens changes its shape continuously to achieve varying focal lengths, similar to the human eye. In one popular design of the fluid an elastic transparent diaphragm that is pressurized by an optically transparent fluid lens is used to achieve variable focusing. The fluid pressure causes the

diaphragm to produce various curved profiles, thus resulting in continuously varying focal lengths. Unlike the conventional variable focal length lenses (such as a zoom lens) where the distances between multiple lens elements are varied, the fluid lens accomplishes variable focusing using a single lens. Because of this significant advantage of the fluid lens compared to a glass lens, a number of studies relating to diaphragm-based liquid-filled lenses have been undertaken in the past.

Shaw and Sun [1], studied the optical properties of different liquid-filled fluid lenses to obtain the best membrane shape. The effect of diaphragm clamping boundary conditions, diaphragm thickness and diaphragm cross-section shape were studied using a non-linear finite element method. Shaw and Lin [2] designed and analyzed an asymmetric diaphragm type fluid lens. By controlling the tilt angle of a pressure ring it was possible to control the light direction or the focal length. Zhang et al. [3] developed a variable focus zoom lens on a chip with a wide field-of-view tuning range using the standard micro-fabrication process. The lens was characterized using an array of LEDs as the object, placed at a fixed distance from the lens. Ahn and Kim [4] proposed a crystalline human eye's lens-like variable focusing lens using square glass diaphragms. The square boundary conditions, however, causes the deflected diaphragm to take a cushion-like shape and thus introduce distortions in the image. Several other researchers have looked into various aspects of the fluid lens, such as lens on a micro-fluidic chip [5-7] and obtaining high zoom ratio and wide tuning range [8].

Several authors used various types of actuation mechanisms for the LFD lens to change the lens focal length. For instance, Gunasekaran et al. [9] used a syringe pump to actuate the fluid lens, Kuwano et al. [10] implemented a stepper motor driven syringe mechanism to change the liquid pressure inside the lens, Ren et al. [11] used a servo motor to squeeze an elastic rubber membrane wrapped around the fluid lens, thus varying the pressure within the lens and Lee et al. [12] developed a fluid lens that was tuned using an electro-magnetically actuated diaphragm pump attached to the main lens chamber. Shaw and Lin [13] developed a novel method to actuate the diaphragm lens by pressurizing an O-ring attached to the fluid lens. A thermal-based fluid actuation for a diaphragm micro-lens of 1.9 mm diameter, where the lens diameter was the aperture as well,

has also been developed [14]. In a recently published work, a feed-back auto-focus control method for the LFD lens was developed [15].

Many of the past research on fluid lenses have been targeted towards the lens design and the development of the actuation mechanisms. The focus quality evaluation of the captured images is less explored. Previous researchers have shown how the fluid lens can be used to capture target images such as bar resolution targets [14] or laser beam spot [10], and the focal length tunability has been demonstrated by capturing images at various focal lengths [9,11]. However, the actual focusing criteria have not been studied in any detail.

In this research, a focus measure criterion for a binary (black-white) target captured through the liquid-filled diaphragm (LFD) lens was determined. Focusing in the LFD lens was achieved using a stepper motor-driven syringe mechanism for the fluid actuation, i.e. injection and withdrawal. The focus measure criterion was verified and tested experimentally.

## II. EXPERIMENTAL SETUP AND TECHNIQUE

### A. Fluid lens and CCD camera

The fluid lens diaphragm is made of an elastic transparent polydimethylsiloxane (PDMS) diaphragm. The PDMS material (Sylgard 184, Dow Corning Corp. Ltd.) was poured in liquid form into a spacer-based mould of 100  $\mu\text{m}$  thickness and baked in the oven for one hour at 80°C. The diaphragm was cut into a square shape and placed at the fluid lens chamber. Fig. 1(a) shows the fluid lens construction. The lens assembly has three layers of polymethylmethacrylate (PMMA) plates, each 3 mm thick. The top layer was used to clamp the diaphragm to the middle layer using eight M-3 bolts. A circular washer was placed on top of the diaphragm to distribute the clamping force radially. This prevents leakage and uneven stress distribution in the lens. The middle layer contains a through-hole chamber of 15 mm diameter and 3 mm depth with a side channel connected to the pump mechanism to withdraw or inject the fluid. The chamber was made using black PMMA to prevent ambient light from entering. The bottom layer was made of transparent PMMA that acts as a base for the middle chamber. A PDMS gasket was sandwiched in-between to prevent fluid leakage when fluid pressure is applied to the diaphragm.

The lens was restricted to operate within the flat to convex shape because a concave shape does not produce a real image on the CCD sensor. When fluid is injected into the chamber the diaphragm convexity increases whereas when fluid is withdrawn from the chamber the convexity decreases. This produces a continuous variation in the focal length in both directions. The bottom layer of the fluid lens assembly was attached to a monochrome CCD camera (CV-M50E, 768 $\times$ 494 pixels, 1/2" sensor) through a 25 mm long extension tube. An aperture of 2 mm diameter was attached at the back of the fluid lens. Fig. 1(b) shows the fluid lens and the CCD camera arrangement.

### B. Fluid lens pump and target rail guide

The overall system setup is shown in Fig. 2. The system comprises two stepper motors (model AS66AAET10, Oriental

Motor Co. Ltd.). One of the motors was used for actuating the pump mechanism while the other was used for moving the binary (black/white) target. A syringe-driven pump mechanism was used for fluid injection and withdrawal using a 3 ml (45 mm long) syringe and a lead screw of pitch 0.5 mm. A fluid dosage precision of 3.3  $\mu\text{l}$  is produced by a linear translation of 50  $\mu\text{m}$  of the syringe piston. A guide rail (model SKR46, THK Co. Ltd.) was used to position the binary target at a distance from the fluid lens front surface ranging from 165 mm to 965 mm.

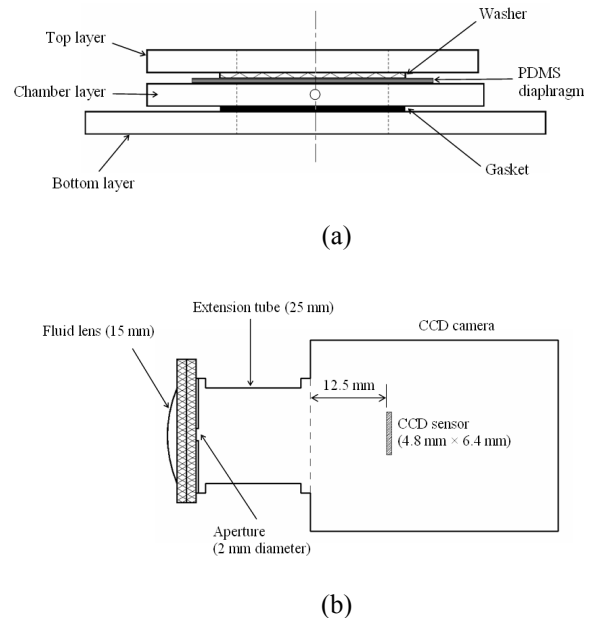


Figure 1. (a) LFD lens construction, (b) LFD lens and CCD camera configuration.

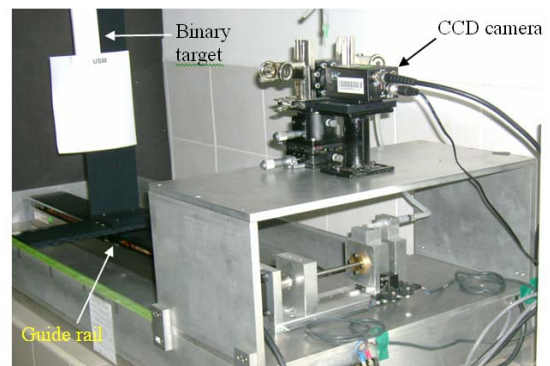


Figure 2. Overall system setup.

### C. System integration

The operation of the fluid lens and the target movement was controlled and integrated using a personal computer with Matlab software as illustrated schematically in Fig. 3. The input images from the CCD camera were sent to the frame grabber (DT3120 – Data Translation Inc.) and processed by a software algorithm to determine the image focus criterion. The control signals were sent through a parallel port interface to

both the pump mechanism motor and the target guide rail motor. As a safety feature, optical sensors (EE-SX671, Omron Electronics Ltd.) were placed to limit the extreme range of the fluid pump and the target guide rail travel. A home position was defined to set the pump to its initial position when required.

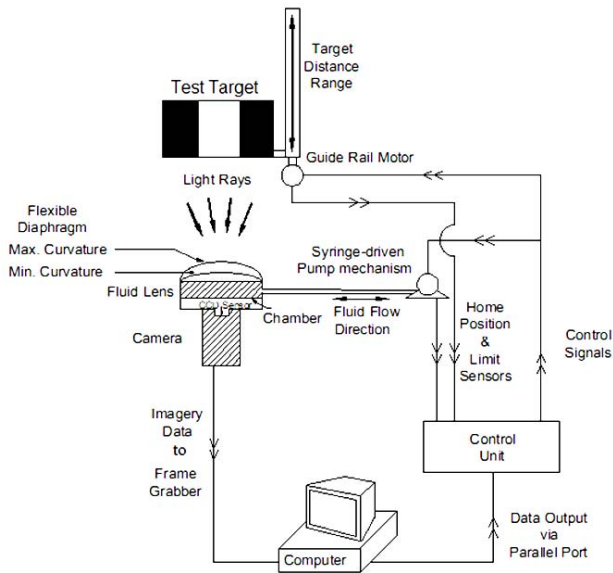


Figure 3. Operational schematic diagram of the system.

#### D. Focus measure criteria

To determine whether an image is in the correctly focused state or otherwise, a focus measure criterion must be established. Usually, the focus measure parameter is derived from the captured image (known as passive focus) to determine the object-to-lens distance. Alternatively, the focus measure parameter can be obtained from auxiliary sources, such as infra-red sensors (known as active focus). Passive focus usually requires high image processing and some prior information about the object in view, such the presence of an edge. However, active focus requires auxiliary devices and costly instrumentation. The human eye is an excellent example of a passive focus device.

In this work, a passive focusing method was implemented by measuring the edge slope width (*ESW*) of the intensity profile along a strip of pixels taken across the black-white transition region in a binary target. A binary target was selected due to the maximum contrast between the bright and dark regions, although the same approach can be used for other targets as long as an intensity transition is present in the image. An algorithm was devised to measure the *ESW* value to determine the best focused image of the target object. Although using *ESW* as a focus measure is considered a basic technique, it produces sufficiently focused images with low image computation. The edge slope width is described in Fig. 4 where the term ‘edge’ refers to the transition between the bright and dark pixels in the image.

The intensity curve shown in Fig. 4 is an ideal case. In practice, an image captured by the LFD lens is much noisier than an image captured by a standard glass lens. This is due to the lower quality of the diaphragm surface finish caused by the molding process. Therefore, it is essential to understand the characteristics of the intensity profile for an image capture by the LFD lens. Fig. 5 shows the various terminologies used to describe the main features of the intensity profile that need to be considered in the focus measure algorithm. The white region of the target object is represented by high intensity value pixels (upper band) while the black region is represented by the low intensity value pixels (lower band). The distance between the end of the upper band region, i.e. slope start  $S_s$ , and the start of the lower band region, i.e. slope end  $S_e$ , is termed the ‘edge slope width (*ESW*)’. *ESW* is the distance that has to be determined by the algorithm. In general, both upper and lower bands have one feature in common, which is the ‘unpredictable region’. For the upper band the ‘unpredictable region’ lies at the beginning of the profile while for lower band it lies at the end. The unpredictable region occurs due to the poor light exposure at the periphery of the target object.

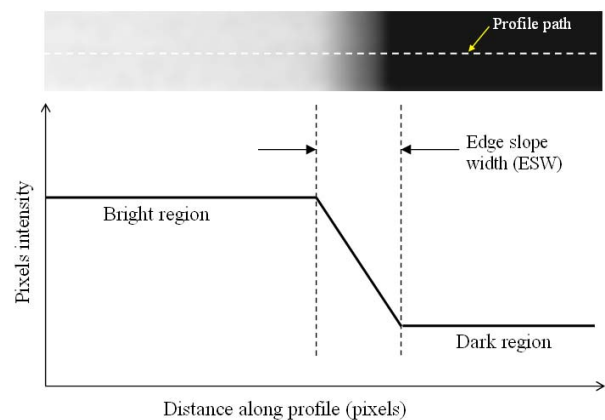


Figure 4. Description of the edge slope width (*ESW*).

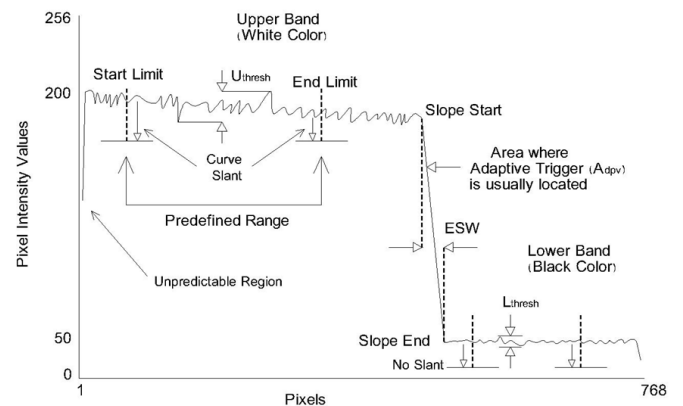


Figure 5. Terminologies used in focus measure using *ESW* across binary target.

The upper band is characterized by a rapid fluctuation in pixel intensity caused by noise, which can be attributed to several factors such as the reflectivity of the target surface, lighting effects and the lens diaphragm quality. The upper band is not only rapidly fluctuating but has a gradual decrease in the mean intensity along the profile, i.e. a slope (slant) in the intensity profile. The reason for the gradual decrease in mean intensity is due to the lighting gradient across the white region of the target. Since the decreasing intensity causes difficulty in locating the slope start point, an upper threshold  $U_{thresh}$  is defined. On the contrary, the lower band is less noisy and the average intensity is more or less constant. This is because the black region is not as reflective as the white and, thus, is not seriously affected by the surface reflectance and non-uniform lighting.

To locate the slope start an algorithm was developed to track the steep downhill of the intensity profile. A flowchart of the algorithm is shown in Fig. 6. Detection of the slope start is done through a sequential pixel-by-pixel intensity comparison at the upper band starting from the ‘end limit’ until the ‘slope start’ is found, i.e. 85% of the slope height is reached. In the pixel comparison, the intensity difference is compared with the upper threshold value  $U_{thresh}$ . The upper threshold value is calculated within the two limits (start and end limits) to avoid the ‘unpredictable’ region and also to reduce the effect of the gradual decrease in mean intensity. This comparison detects a slope start point when the difference in pixel intensity becomes larger than the upper threshold. The purpose of the threshold is to avoid false downhill caused by the fluctuating values in the upper band. Four pixels located at 10 pixels apart along the profile are compared at once with the threshold value to ensure a reliable prediction of the slope start. The first of the four pixels is a dynamic pixel, i.e. pixel location that varies from the current location ‘1’ to pixel location ‘14’. Implementation of a dynamic comparison compensates the effect of the upper band slope and the fluctuating intensity values. For the lower band the slope end point is found by detecting the steep uphill and a static pixel comparison is implemented since the intensity fluctuation is small in the lower band. Static pixel comparison means a fixed pixel location as opposed to a dynamic comparison where the pixel location varies according to the activation of an adaptive trigger. An adaptive trigger is used to initiate the dynamic comparison, i.e. when the position of the pixels being compared reach about 85% of the slope height then the comparison is restarted and the distance between the two subtracted pixels is changed.

A description of the algorithm shown in Fig. 6 and the related links in Fig. 7 and Fig. 8 are as follows:

1. The algorithm starts by first receiving an image from the main program.
2. A  $5 \times 5$  average filter is applied to suppress noise in the image.
3. A line profile is taken from the left to the right, i.e. column 1 to 768 and row 10 (counted from top in the captured image).

4. The upper band threshold is found by subtracting the minimum and maximum pixel intensity values within a predetermined range of pixels (between start and end limits). The same is done to find the lower band threshold.
5. Search for the edge slope start point begins right after the end limit, i.e. by comparing the current pixel (reference pixel) with four other pixels ahead (first pixel being dynamically chosen from 1 to 14 pixel in position while the rest are fixed at the following positions: 15, 25 and 35). If all of the four pixel intensities have lower or equal value than the threshold then it is a slope start.
6. Adaptive trigger variable is used to activate the dynamic method when the current pixel intensity becomes equal to the adaptive trigger value. Adaptive trigger value is equal to 85% of the slope height intensity value.
7. The dynamic pixel is updated when the current pixel intensity value becomes less than that of the adaptive trigger value. Only 15 iterations are allowed.
8. Search for slope end is done by a simpler method by comparing the current pixel with the pixels lying at 4, 15, 25 and 35 pixels before it; when all of them have a higher value than the threshold then it is a slope end.
9. ESW value is calculated by subtracting the slope start value from slope end value.

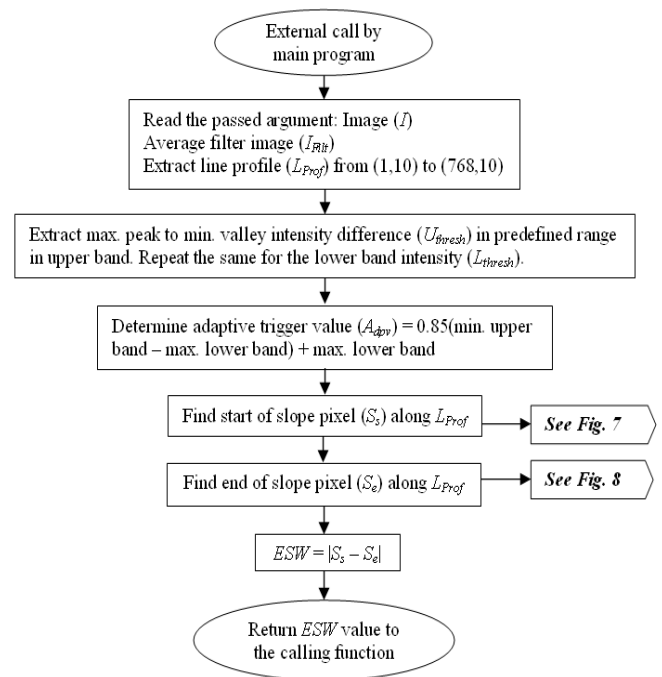


Figure 6. Flow-chart of the algorithm used to find the ESW.

### III. RESULTS AND DISCUSSION

#### A. Optimum ESW value for a focused image and ESW trend graph

An image is considered to be in correct focus when the *ESW* value is at a minimum. Such a value corresponds to a sharp edge, thus indicating a high-contrast image. Thirty test trials were conducted to assess the algorithm and find the appropriate *ESW* value for a focused image. In each test the target was positioned at a known distance from the fluid lens and the focal length was tuned by the pump mechanism until a minimum a *ESW* value was obtained. It is shown experimentally in Fig. 9 that for focused images of a binary target at different distances an *ESW* of either 11 or 12 pixels represents a well-focused image. Fig. 10 shows how the *ESW* value gradually changes when the image transitions from an unfocused image to a focused image and then back to an unfocused image during the tuning of liquid volume in the diaphragm lens.

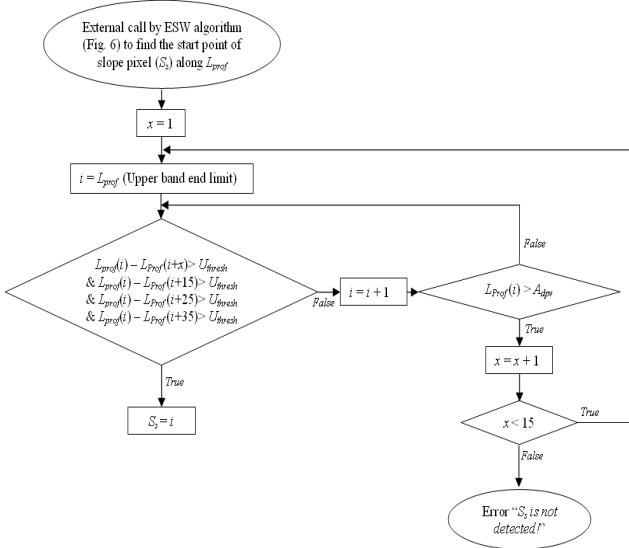


Figure 7. Flow-chart of the algorithm used to find slope start point.

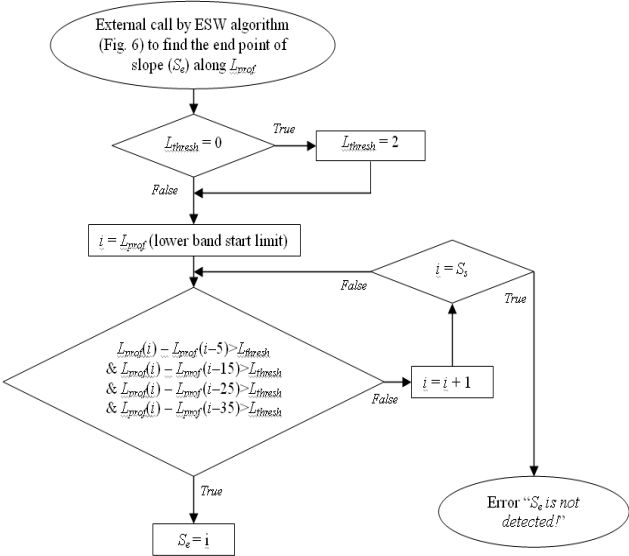


Figure 8. Flowchart of the algorithm implemented to find the slope end ( $S_e$ ).

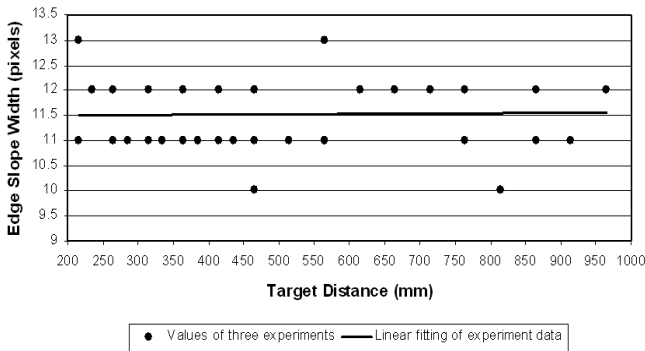


Figure 9. Values of ESW for various target object distances.

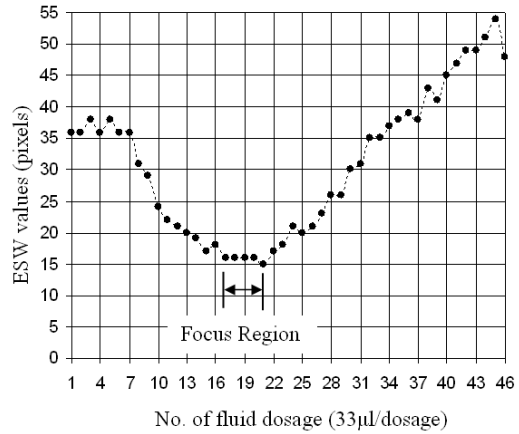


Figure 10. Trend of ESW values for a target placed at 215 mm.

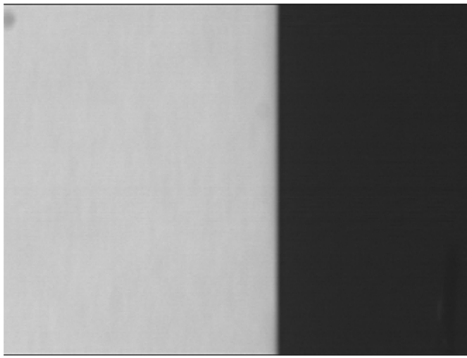
#### B. Consistency of ESW measurement

In order to test the consistency of the edge slope width criterion for focusing, several experiments were conducted to show the variance in the *ESW* values with respect to lighting effects. Two cases were considered in the experiments:

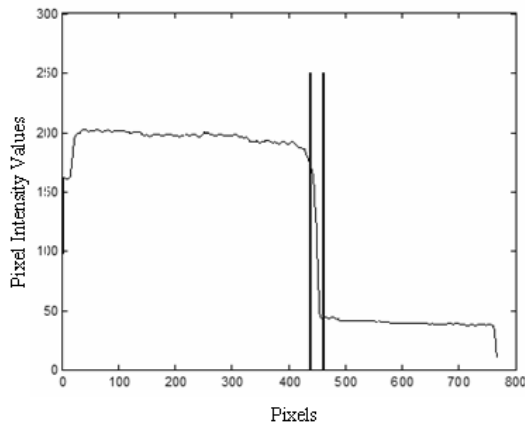
- 1) Change in lighting condition, where the target object is exposed to ambient room lighting and projector lamp.
- 2) Effects of projector lamp and CCD flickering.

#### Case I:

A comparison of capturing an image with and without ambient lighting was conducted for this purpose. An aperture of 5 mm, instead of 2 mm, was used to amplify the effect of light on the focus measure criterion. Due to the larger aperture the minimum *ESW* value varies as well, since large apertures introduce optical degradation. The experiment settings were as follow:



(a)



(b)

Figure 11. Target captured during exposure to projector lamp only (a) real image of the target, (b) intensity values, ESW value = 24 pixels.

1. Three images were taken of a binary target, placed at a distance of 215 mm from the fluid lens, with the same fluid lens focal length.
2. The lighting parameter was changed in the experiment: at the first trial only the projector lamp was switched on (Fig. 11) while at the second trial the ambient light was also switched on.

The results showed that the presence of ambient light affects the *ESW* value by about 20% (5 pixels). Since ambient lighting affects the consistency of the *ESW* value, alteration in ambient lighting is undesirable. The effect of using 5 mm over 2 mm aperture size will be discussed in the coming sections.

#### Case II:

The images captured repeatedly by the CCD camera was found to undergo changes in intensity values although there is neither alteration to the fluid pump motor rotation nor to the target object lighting. The changes in intensity values of the image are due to two factors:

- 1) Lighting operation frequency

The lighting used for illumination from a projector is normally restricted to a range of operational frequency.

Since this frequency causes a fluctuation in the light intensity, repeated images captured do not all have identical lighting exposure.

- 2) Camera CCD flicker

Flicker is a measure of the percentage of the difference between two fields in the CCD sensor pixels array. According to the data sheet of the CCD manufacturer a 2% flicker is the value for the currently used camera. Therefore, due to the presence of flicker the transmission of light through the sensor pixels array is not the same each time a new image is captured.

The above two factors cause a change in the intensity values of the images captured for the same setting. This, in turn, affects the *ESW* measurement algorithm for determining the *ESW* value. Thus, to study the effect of such factors, multiple images were captured under the same camera, lighting and target object settings to evaluate the amount of fluctuations in the *ESW* measurement. The experiments were done at four target object distances: 365 mm, 565 mm, 765 mm and 965 mm. At each target object distance eighteen images were captured. The aperture used in this experiment is 2 mm in diameter.

The results show that there were some fluctuations in the slope width measurement although no parameters were varied during the trials. A variation of 3 pixels (from 11 to 13 pixels) in the slope width measurement can be detected which shows the sensitivity of the slope width measurement to light frequency and CCD flicker.

#### IV. CONCLUSION

A liquid-filled diaphragm (LFD) lens was successfully fabricated and integrated in a fluid actuation system along with a moving target system. Images of black and white target were captured by the LFD lens and were analyzed to formulate a focus measure algorithm based on the pixel intensity values. The intensity fluctuation, lighting effect and other uncertainties present in the intensity profile were overcome by the focus measure algorithm. Experimental trials verified the working of the algorithm and showed that there exists a range of edge slope width values that correspond to a focused image. It was shown experimentally that alteration of ambient light affects the *ESW* value by about 20%. Also, due to the lighting frequency and the CCD flicker frequency the focus measure algorithm did not produce the same *ESW* values for repeated image capturing operations.

It was shown earlier that a value of 11 or 12 of the edge slope width corresponds a focused image. Therefore, this value can be used to find the focused image provided that focus measure operation is performed under predefined working environment (i.e. constant lighting and system setup) and as long as the image of a binary target is available in the field-of-view for the *ESW* measurement.

#### ACKNOWLEDGMENT

The authors would like to thank the Ministry of Science, Technology and Innovation (MOSTI), Government of Malaysia, for the offer of the Science Fund Grant (no. 03-01-05-SF0121) that has resulted in this work.

#### REFERENCES

- [1] D. Shaw and T. E. Sun, "Optical properties of variable-focus liquid-filled optical lenses with different membrane shapes," *Optical Engineering*, vol. 46 no. 2, pp. 024002, 2007.
- [2] D. Shaw and L. Chih-Wei, "Design and analysis of an asymmetrical liquid-filled lens", *Optical Engineering*, vol. 46 no. 12, pp. 123002, 2007.
- [3] D. Y. Zhang, N. Justis, Y. H. Lo, "Fluidic zoom-lens-on-a-chip with wide field-of-view tuning range," *IEEE Photonics Tech. Lett.*, vol. 16, no. 10, pp.2356-2358, 2004.
- [4] S. H. Ahn, Y. K. Kim, "Proposal of human eye's crystalline lens-like variable focusing lens," *Sensors and Actuators A*, vol. 78, pp. 48-53, 1999.
- [5] D. Y. Zhang, N. Justis, Y. H. Lo, "Integrated Fluidic Lenses and Optic Systems," *IEEE J. of Selected Topics in Quantum Electronics*, vol. 11, no. 1, pp. 97-106, 2005.
- [6] J. Chen, W. Wang, J. Fang, K. Varahramyan, "Variable-focusing microlens with microfluidic chip," *J. Micromech. Microeng.*, vol. 14, pp. 674-680, 2004.
- [7] M. Agarwal, R. A. Gunasekaran, P. Coane, K. Varahramyan, "Polymer-based variable focal length microlens," *J. Micromech. Microeng.*, vol. 14, pp. 1665-1673, 2004.
- [8] D. Y. Zhang, N. Justis, Y. H. Lo, "Fluidic adaptive zoom lens with high zoom ratio and widely tunable field of view," *Optics Communications*, vol. 249, pp. 175-182, 2005.
- [9] R. A. Gunasekaran, M. Agarwal, A. Singh, P. Dubasi, P. Coane, K. Varahramyan, "Design and fabrication of fluid controlled dynamic optical lens system," *Optics and Lasers in Engineering*, vol. 43, pp. 686-703, 2005.
- [10] R. Kuwano, T. Tokunaga, Y. Otani and N. Umeda, "Liquid Pressure Varifocus Lens," *Optical Review*, vol.12 no. 5, pp. 405-408, 2005.
- [11] H. Ren, D. Fox, P. A. Anderson, B. Wu and S. T. Wu, "Tunable-focus liquid lens controlled using a servo motor," *Optics Express*, vol. 14 no. 18, pp. 8031-8036 (2006).
- [12] S.W. Lee and S. S. Lee, "Focal tunable liquid lens integrated with an electromagnetic actuator," *Appl. Phys. Lett.* vol. 90, pp.121-129, 2007.
- [13] D. Shaw, C. W. Lin, "Design of O-ring driven liquid-filled lens," *Proceedings of the 35<sup>th</sup> International MATADOR conference*, pp. 63-66, June 2007.
- [14] W. Wang, J. Fang, "Design, fabrication and testing of a micromachined integrated tunable microlens," *J. Micromech. Microeng.*, vol. 16, pp. 1221-1226, 2006.
- [15] S. J. Abdullah, M. M. Ratnam and Z. Samad, "Error-based autofocus system using image feedback in a liquid-filled diaphragm lens", *Optical Engineering*, vol. 48 no. 12, pp. 123601(1)-123601(9), 2009.